Journal of Ceramic Processing Research. Vol. 5, No. 3, pp. 281~286 (2004)

J O U R N A L O F
Ceramic Processing Research

Fabrication and mechanical properties of Si_3N_4/SiC/TiAgCu multilayered nano-composites

Do Won Seo and Jae Kyoo Lim*

Research Center of Industrial Technology, Engineering Research Institute, Faculty of Mechanical & Aerospace System Eng., Chonbuk National University, Jeonju 561-756, Korea

Two-layered Si_3N_4/SiC nano-composites with 20 vol.% SiC have been fabricated by two-step sintering of a powder mixture of α-Si_3N_4 and carbon powder with a mean size of 13 nm, and 5 wt.% Y_2O_3. Nano-sized SiC particles were formed through reactions: carbon and surface SiO_2 on the Si_3N_4 particles, and carbon and Si_3N_4 particles. To combine the specific advantages of nanoscale ceramics with that of metals, they are often used together within one composite component. In this study, the fabrication and mechanical properties of a nanoscale SiC layer brazed with a Ti active alloy were investigated. It was shown that, with a variation of strain rate, the joints have a bending strength of 310-380 MPa, and the deflection of the interlayer increases with increasing strain rate. The fracture types are classified into three groups; cracks grow into the metal-brazing filler layer, the ceramic-brazing filler layer or inside the ceramic.

Key words: brazing, nanoscale SiC, TiAgCu, mechanical properties, sintering.

Introduction

Ceramic-metal joining is important for the application of ceramics in structural components. The fracture strength of the ceramic-metal joint is, however, influenced by the residual stresses and the stress concentrations caused by the difference between the thermal expansion coefficients and between the elastic moduli. Regarding the material combinations and the method of joining, many experimental studies have been conducted [1]. As engineering ceramics, silicon nitride (Si_3N_4) ceramics and composites made from Si_3N_4, no matter whether they are dense or porous, are potential materials for use at high temperatures. Various processing techniques have been developed to fabricate Si_3N_4 ceramics and composites from Si_3N_4 for structural or functional applications [2]. Porous Si_3N_4 ceramics with a microstructure of rod-like β-Si_3N_4 grains shows superior mechanical properties, such as high strength, good thermal shock resistance, and high strain and damage tolerance [3]. Thus, an α to β phase transformation with little or no densification is preferred when fabricating porous Si_3N_4 ceramics by sintering. Because densification by particle rearrangement usually occurs before the phase transformation, and the reconstructive α to β phase transition also provides a driving force for densification, ceramics with a porosity higher than 50% are difficult to obtain by sintering at high temperature with a full phase transformation [4]. Thus how to increase the porosity while keeping a fine pore size, good shaping behavior and sinterability is still an unresolved problem in the fabrication of porous ceramics.

In 2001, Yang *et al*. [5] have demonstrated a successful means to fabricate porous Si_3N_4 ceramics with high porosity through sintering a powder mixture of Si_3N_4 and 1-5 vol.% (0.7-3.4 wt.%) carbon together with a sintering aid. Reactions between SiO_2 or Si_3N_4 and the added carbon powder occur in the ceramic green body [6]:

$$3C(s) + SiO_2(s) \rightarrow SiC(s) + 2CO(g) \quad (1)$$

$$3C(s) + Si_3N_4(s) \rightarrow 3SiC(s) + 2N_2(g) \quad (2)$$

The critical temperature for the conversion from Si_3N_4 to SiC has been estimated as 1435°C, and the formation of SiC starts between 1400 and 1450°C [7]. These reactions have also been used to fabricate SiC based composites [8, 9]. Reaction (1) occurs more easily than does reaction (2) in the Si_3N_4-SiO_2-C system [10]. After the SiO_2 on the Si_3N_4 surface is consumed, the remaining carbon reacts with Si_3N_4, according to reaction (2). The Si_3N_4 grains would then be bonded together by the reaction-formed SiC particles located at the grain boundaries, and the shrinkage of Si_3N_4 ceramics was thus decreased. On other hand, these reactions result in a weight loss of about 32% theoretically, simultaneously through these reactions during sintering. In another words, the porosity can partly be adjusted by the amount of carbon.

In the present study, Si_3N_4/SiC nanocomposites with 20 vol.% SiC were fabricated in free surface layers by

*Corresponding author:
Tel : +82-63-270-2321
Fax: +82-63-270-2460
E-mail: jklim@chonbuk.ac.kr

the carbothermal reaction between Si_3N_4 and carbon. The effect of the carbon addition on the sinterability, microstructural development and mechanical properties were investigated. In addition, four-point bending tests were conducted for Si_3N_4/SiC brazed to 304 stainless steel (SS 304) joints with various strain rates, and the variation in the deflection of the Cu interlayer, at the center of the specimen, was studied at room temperature.

Experimental

Si_3N_4/SiC nanocomposites were fabricated at the surface layers using the reaction process between Si_3N_4 and carbon powders. The powders used were high purity Si_3N_4 (SN-E10, UBE Industries Ltd, Tokyo, Japan; α ratio: >95%, mean particle size: 0.5 μm, main impurities by weight: O=1.6%; C<0.2%; Cl, Fe, Ca and Al_2O_3<50 ppm), carbon (No. 2600, Mitsubishi Chemical Corp., Tokyo, Japan; mean particle size: 13 nm) and as sintering aid Y_2O_3 powder (99.9% purity, Kojundo Chemical Lab. Co, Ltd, Sakado, Japan). For the fabrication of Si_3N_4/SiC nanocomposites with 20 vol.% SiC, which is the volume fraction of the solid parts of Si_3N_4 and SiC in the composites, the following compositions of powder mixture was used: 89.63 wt.% Si_3N_4, 5.37 wt.% carbon, calculated according to the reactions (1) and (2). 5 wt.% Y_2O_3 as the sintering additive was added in. After sintering, the resultant SiC content may somewhat deviate from the calculation due to the difference in weight loss of the individual components. The above powder mixture was firstly wet-milled in methanol for 24 h using an high-purity Si_3N_4 media. Then, the slurry was dried and sieved through a 250 μm screen. The powder mixture was then uniaxially pressed at 10 MPa to form rectangular bars measuring 50×40×20 mm. Some of the samples were then cold isostatic pressed (CIPed) under a pressure of 200 MPa. The green bodies were placed in a BN-coated graphite crucible. A pre-sintering of 1600°C/4 hr in an argon atmosphere at a gas pressure 0.6 MPa was used to obtain SiC particles through the reactions. Then the samples were sintered in a graphite resistance furnace at 1650, 1750 and 1900°C for 2 hr in a nitrogen atmosphere at a gas pressure 0.6 MPa with a temperature ramp rate of 15 $Kmin^{-1}$. This two step method enhances the formation of SiC and the sintering of the Si_3N_4 matrix.

The bulk density and open porosity of the sintered products was measured by the Archimedes displacement method using distilled water. The porosity was calculated from the relative density and theoretical density, which was calculated by the rule of mixtures. Crystalline phases in sintered samples were identified by X-ray diffraction (XRD, D/MAX-2000, Rigaku Co. Ltd, Tokyo, Japan) analysis at 40 kV and 100 mA using CuKα radiation, a step width of 0.02° and a counting time of 0.3 s. The microstructures were characterized by scanning electron microscopy (SEM, S-4700, Hitachi Ltd, Tokyo, Japan).

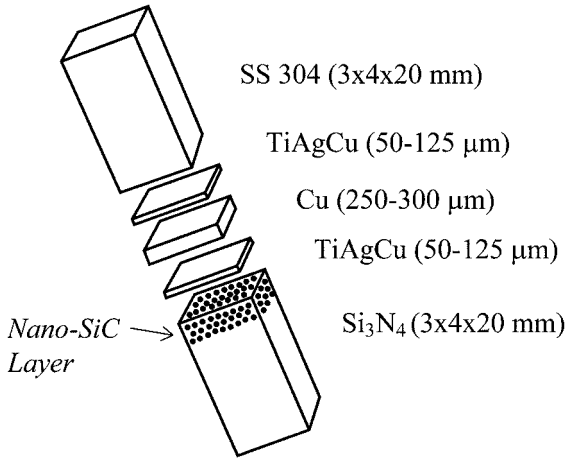

Fig. 1. Specimen configuration.

The sintered Si_3N_4 and 304 stainless steel were joined by an active metal vacuum-brazing method at 800-820°C. A copper sheet was used as the interlayer and TiAgCu alloy (Cusil-ABA, WESGO Metals, San Carlos, USA) was used as the brazing filler metal. Si_3N_4 specimens were cut into 3×4×20 mm bars. The bond surface of each bar was ground to an average surface roughness of about 0.5 μm, and the faces of the 304 stainless steel were finished with a 1200 grit SiC emery paper and macro-etched to remove any oxide film. The thickness of the Cu interlayer and TiAgCu brazing filler layers were 250-300 and 50-125 μm respectively, as shown in Fig. 1. Four-point bending test procedures were conducted in accordance with the American Society for Testing and Materials (ASTM) standard E855-90 [11]. The interface was set at the midpoint of the span. The test procedures were performed by an hydraulic universal test machine (8516, Instron Co., Canton, USA) with a 10 kN load cell. The outer span distance was 30 mm and the inner one was 10 mm. The nominal bending strength, σ_{b4}, ignoring the material discontinuity was calculated from the following equation [11]:

$$\sigma_{b4} = 3P(L-l) / 2bh^2 \quad (3)$$

where P is the maximum load (fracture load), L is the outer span, l is the inner span, b is the specimen width and h is the specimen height.

The tests were carried out at various longitudinal normal strain rates, rate $\dot{\varepsilon}$ =8.2×10^{-6}, ×10^{-5}, ×10^{-4}, ×10^{-3} and ×10^{-2} s^{-1}, to evaluate the effect of strain rate on the strength of the joint at room temperature. To evaluate the strains that accompany the plastic deformation in localized areas at the edge of the beam, two strain gages were attached near the joint interfaces at the Si_3N_4 and SS 304 sides. Each strain gage was attached on the lower side opposite the applied tensile

load and its gage length was 2 mm.

Results and Discussion

Synthesis properties of Si_3N_4/SiC nanocomposites

According to reactions (1) and (2), assuming 1.6% oxygen on the surface of raw Si_3N_4 particles, the weight loss after sintering would be 9.28% theoretically for a composite with 20 vol.% SiC. The measured weight loss, relative density and porosity of sintered bodies are shown in Table 1. The weight loss of samples sintered at 1650 and 1750°C was lower than the theoretical value, while that of samples sintered at 1900°C was almost the same. The low weight loss at low temperatures of 1650°C and 1750°C arises from the fact that a mass of the carbon remained after the sintering and the reaction was incomplete, indicating that it need a higher temperature to transform carbon to SiC for the bulk samples.

The shrinkage of all samples after sintering was within 1%, indicated that the original dimensions of the powder compact remain virtually unchanged during sintering. The low shrinkage indicated a significant effect of the carbon addition on the densification behavior, and the shrinkage was apparently restrained by the reaction between carbon and Si_3N_4. The densification of Si_3N_4 ceramics using Y_2O_3-Al_2O_3 oxide as sintering additives begins at temperature above 1400°C [12], at which a glass phase forms and particle rearrangement is the main densification mechanism. The reaction between carbon and Si_3N_4 (reaction (2)) also begin at this temperature, and prior to it, the reaction between carbon and surface SiO_2 (reaction (1)) begins. The occurrence of these reactions was at the surface of Si_3N_4 particles, and the reactant was located either at their surfaces or between the Si_3N_4 particles, which results in a reaction bonding between Si_3N_4 grains. It is well known that the glass phase plays an important role in particle rearrangement of Si_3N_4, and the densification of Si_3N_4 ceramics by liquid phase sintering is dependent on the characteristics of this glass phase, such as amount and viscosity [12]. At a relatively low temperature, lower than 1600°C, the viscosity of the glass phase is high, so the densification is limited [12]. As the reactions begin almost simultaneously with the glass formation, the bonding of the Si_3N_4 particles by the reaction-formed SiC particles is very likely to act as an obstacle to the movement of Si_3N_4 particles and restrains their rearrangement. With an increase in sintering temperature, the increased viscosity of the glass phase produces a tendency for densification; however, as the bonding among Si_3N_4 grains was strong, hardly any grain rearrangement took place. Finally a low sintering shrinkage (within 1%) and a high porosity after sintering were the result. This method of producing porous ceramics can be defined as a restrained sintering by reaction bonding (RSRB). Due to the low shrinkage and high weight loss during the reactions mentioned above, the relative densities after sintering were even lower than the relative densities of the green bodies. With a degree of CIPing, the final relative densities were adjustable from 35 to 50%. The pores were mostly of open type. Compared with the density obtained by weight: volume ratio, the difference between the resultant density was within 1%, indicating that the results obtained from the Archimedes method were believable.

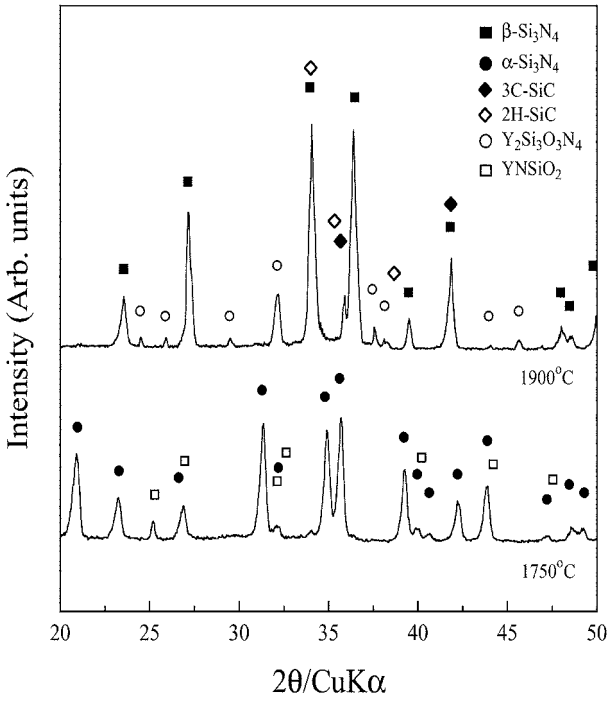

Fig. 2. XRD patterns of sintered samples at 1750 and 1900°C.

Table 1. Synthesis properties of sintered Si_3N_4/SiC nanocomposites.

Sample	Relative density of green body	Sintering temperature (°C)	Weight loss (%)	Relative density after sintering	Total porosity	Open porosity
20% SiC	0.397	1650	7.3	0.392	0.612	0.610
		1750	7.8	0.381	0.616	0.614
		1900	9.5	0.359	0.640	0.639
20% SiC with CIP	0.551	1650	7.2	0.490	0.510	0.494
		1750	7.7	0.491	0.511	0.509
		1900	9.6	0.494	0.505	0.443

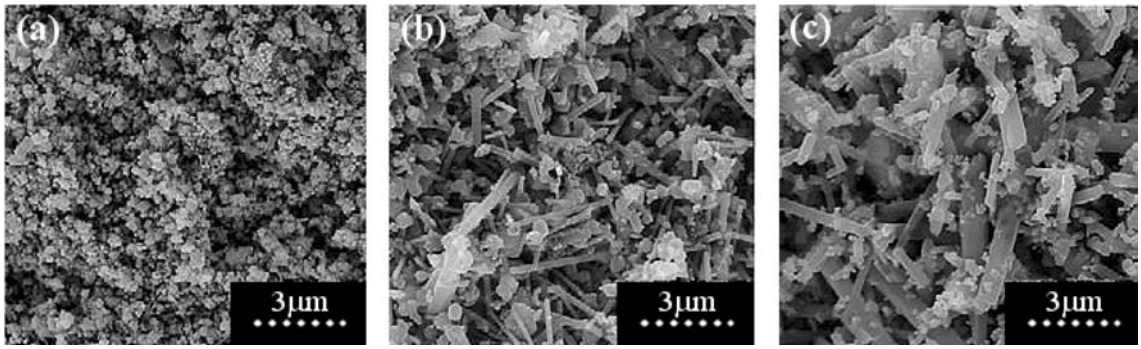

Fig. 3. SEM micrographs of Si_3N_4/SiC nanocomposites. (a) green body, (b) sintered at 1750°C, (c) sintered at 1900°C.

The XRD patterns from samples sintered at 1750 and 1900°C are shown in Fig. 2. These show that the reaction between α-Si_3N_4 and carbon could not go to completion when sintered at 1750°C, so that a mass of α-Si_3N_4 remained in the sample. In addition, the existence of carbon would also prohibit the α to β-Si_3N_4 phase transformation. At the high temperature of 1900°C, the reaction went to completion, so that β-Si_3N_4, 3C-SiC and 2H-SiC could be detected. Beside the Si_3N_4 and SiC phases, some other phases such as $Y_2Si_3O_3N_4$ and $YNSiO_2$ formed from the sintering additive. Surface SiO_2 on the Si_3N_4 particles and Si_3N_4 were also detected. Due to the amorphous type of the C starting reactant there is no peak in the patterns from this material.

Micrographs of the green body exhibited very fine particles composed of fine α-Si_3N_4 particles and nanoscale carbon particles as shown in Fig. 3(a). At 1900°C, the transformation occurs from α-Si_3N_4 to β-Si_3N_4 and the β-Si_3N_4 can be easily identified in the microstructure due to its elongated grain morphology. The SiC particles should be very fine due to the use of carbon particles with a size of 13 nm. When heated at 1750°C, fine β-Si_3N_4 elongated grains were seen in Fig. 3(b), however, equiaxed α-Si_3N_4 and carbon particles still remained due to the incomplete reaction, which was also indicated by the XRD results. With increasing the sintering temperature to 1900°C, grain growth of β-Si_3N_4 was observed, and no carbon particles can be seen in Fig. 3(c). Similar to the dense Si_3N_4/SiC nanocomposites, a high SiC content resulted in restrained β-Si_3N_4 grain growth [13]. It can be seen that the SiC particles obtained from the reaction between carbon and Si_3N_4 have a very fine size of about 100-200 nm, which was almost independent of the sintering temperature. The SiC particles located around the β-Si_3N_4 grains which are suggested to inhibit the densification of the Si_3N_4 matrix as analyzed in Table 1.

Mechanical properties of Si_3N_4/SiC/TiAgCu composites

The relations between the bending strength and the longitudinal normal strain rate in the Cu interlayer

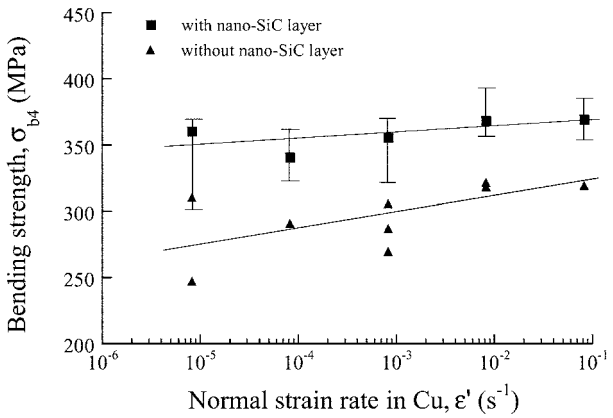

Fig. 4. Strength distribution of brazed joints with various strain rates.

obtained from the four point bending tests at room temperature are shown in Fig. 4. The bending strength of the brazed joints including the nanoscale SiC reaction layer was distributed in the range of 310-380 MPa. The strength shows an almost linear increase from $\dot{\varepsilon} = 8.21\times10^{-6}$ up to 8.21×10^{-2} s^{-1}. This result is in reasonable agreement with other research works for Ti alloys and other metals [14]. Further, the strength of composites brazed with a nanoscale SiC layer increased in comparison with a previous study [15], which was made on Si_3N_4-SS 304 brazed joints without a nanoscale SiC reaction layer. This is due to an increase in the reaction area caused by ultra-fine carbon particles. The specimens mainly fractured along the interfaces between the Cu interlayer and the SS 304 metal side as shown in Fig. 5. The cracks initiated at the reaction layer of the SS 304-TiAgCu filler, so the fracture behavior was similar to metals. The deflection level of the Cu interlayer at maximum strength generally increased with increasing strain rate. This result might be influenced by increasing the strength with higher loading rates in the relatively high strain rate region. The downward displacement of the specimens, increased with increasing applied load.

The variation in the maximum localized strain with various strain rates near the joint interfaces of the Si_3N_4 and SS 304 is illustrated in Fig. 6. These curves show

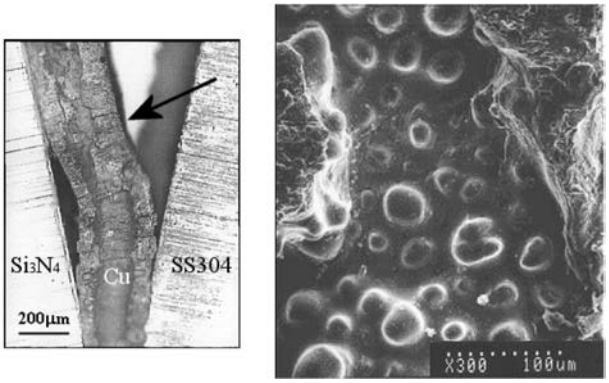

Fig. 5. SEM micrographs of a brazed joint after failure.

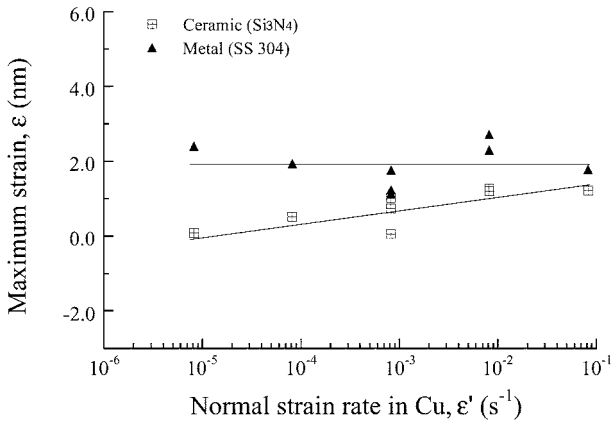

Fig. 6. Maximum strain of brazed joints with various strain rates.

the strains at maximum strength, that is, at fracture. The tensile load was applied to strain gages perpendicular to the ceramic/metal interface. The strain level on the metal side remained almost constant with an increase in strain rate. However, the localized strain on the ceramic side showed a tendency that gradually increased with increasing strain rate. At relatively higher strain rates, the gap in the strain levels between the Si_3N_4 and SS 304 was small. This may be due to the high loading rate applied to specimens. Individual deformation of the ceramic and metal seemed to be impossible because the two materials were joined with brazing alloy and a high loading rate was applied. In the relatively lower strain rate region, the value of the strain in the Si_3N_4 was almost zero, but the value of the strain in the SS 304 slightly increased because of the characteristics of this relatively ductile metal.

The fracture shapes are classified into three groups as shown in Fig. 7. When the strain rate $\dot{\varepsilon}=8.2\times10^{-6}$, $\times10^{-4}$, $\times10^{-3}$ and $\times10^{-2}$ s^{-1} at room temperature, the crack initiated mainly at the Cu interlayer/SS 304 interface (Fig. 7(a)). In the rare case of $\dot{\varepsilon}=8.2\times10^{-4}$, the crack initiated either at the Cu interlayer/Si_3N_4 interface (Fig. 7(b)) or first at the Cu interlayer/Si_3N_4 interface, and then the crack path changed from the interface to inside the Si_3N_4 and it finally resumed its course to the interface (Fig. 7(c)).

Conclusions

Si_3N_4/SiC nanocomposites with 20 vol.% SiC were fabricated at free surface layers by the carbothermal reaction between Si_3N_4 and carbon. Four-point bending tests were conducted for brazed Si_3N_4/SiC to 304 stainless steel joints. Results showed that controlled porosity is obtainable by varying the carbon content and green density. The samples exhibit microstructures that are composed of fibrous Si_3N_4 grains and nanosized SiC particles, a fine pore size, and a good permeability due to the high porosity. The bending strengths increased linearly with increasing strain rate at room temperature and were distributed from 310 to 380 MPa. The strength of composites brazed with a nanoscale SiC layer increased in comparison with brazed joints without a nanoscale SiC reaction layer.

Acknowledgements

This work was supported by grant No. R08-2003-000-10289-0 from the Basic Research Program of the Korea Science & Engineering Foundation.

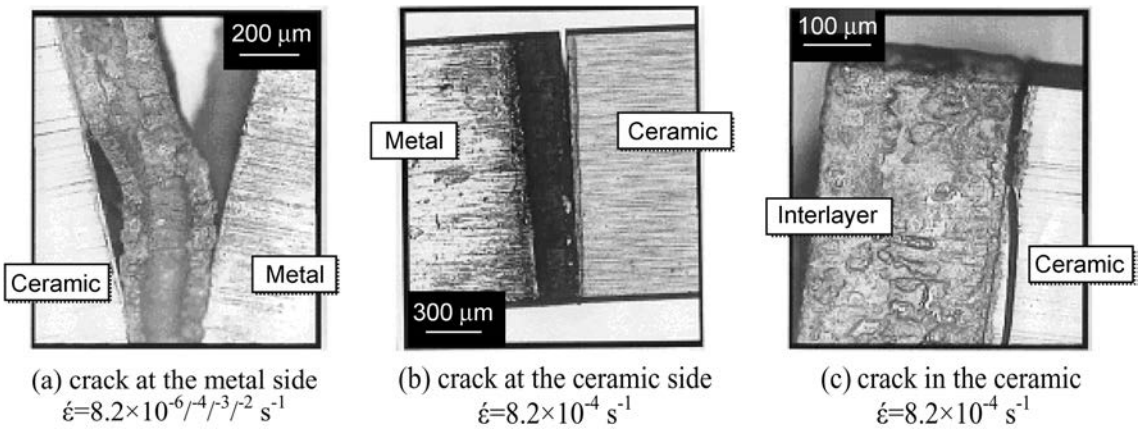

Fig. 7. Classification of fracture shapes.

References

1. K. Suganuma, T. Okamoto, and K. Kamachi, J. Mater. Sci. 22 (1987) 2702-2706.
2. J.B. Davis, A. Kristoffersson, and W.J. Clegg, J. Am. Ceram. Soc. 83[10] (2000) 2369-2374.
3. G.J. Zhang, J.F. Yang, and T. Ohji, J. Am. Ceram. Soc. 84[6] (2001) 1395-1397.
4. C. Kawai and A. Yamakawa, J. Am. Ceram. Soc. 80[10] (1997) 2705-2708.
5. J.F. Yang, G.J. Zhang, and T. Ohji, J. Am. Ceram. Soc. 84[7] (2001) 1639-1641.
6. Y.S. Oh, W.S. Cho, C.S. Kim, D.S. Lim, and D.S. Cheng, J. Am. Ceram. Soc. 82[4] (1999) 1076-1078.
7. D. Sciti, J. Vicens, N. Herlin, J. Grabis, and A. Bellosi, J. Ceram. Process. Res. 5[1] (2004) 40-47.
8. G.J. Zhang, Y. Beppu, T. Ohji, and S. Kanzaki, Acta Mater. 49 (2001) 77-82.
9. G.J. Zhang, J.F. Yang, Z.Y. Deng, and T. Ohji, J. Ceram. Soc. Jpn. 109 (2001) 45-48.
10. J.F. Yang, G.J. Zhang, N. Kondo, and T. Ohji, Acta Mater. 50 (2002) 4831-4840.
11. Annual Book of ASTM Standards, Metals Test Methods and Analytical Procedures, Vol. 03.01, E855-90, ASTM, Philadelphia, 1993, pp. 760-767.
12. J.F. Yang, T. Ohji, and K. Niihara, J. Am. Ceram. Soc. 83[8] (2000) 2094-2096.
13. J.F. Yang, T. Sekino, Y.H. Choa, K. Niihara, and T. Ohji, J. Am. Ceram. Soc. 84[2] (2001) 406-412.
14. M. Jain, M.C. Chaturvedi, and N.L. Richards, Mater. Sci. Eng. A138 (1991) 205-211.
15. D.W. Seo and J.K. Lim, KSME Int. J. 16[9] (2002) 1078-1083.